

An Overview on the Facile and Reversible Cations Intercalation in Nickel-Hexacyanoferrate Open Framework

Michela Ciabocco¹, Mario Berrettoni^{1,*}, Silvia Zamponi², Reno Spinosi² and Paolo Conti²

¹ Dipartimento di Chimica Industriale “Toso Montanari”, UOS, Campus di Rimini, Università di Bologna, Rimini, Italy

² Scuola di Scienze e Tecnologie, Università di Camerino, Camerino, Italy

*E-mail: mario.berrettoni@unibo.it

Received: 14 February 2018 / Accepted: 23 March 2018 / Published: 10 May 2018

The paper reports a detailed study about the influence of the electrolyte composition in nickel-hexacyanoferrate (NiHCF) electrochemical behavior. Shapes and positions of the CV waves are strongly related to the cation of the supporting electrolyte, which undergoes intercalation/de-intercalation during the redox process. The electrochemical behavior of NiHCF has been characterized in different electrolyte solutions containing either pure monovalent or trivalent metal nitrates. Nickel-hexacyanoferrate permits the reversible insertion of a wide variety of monovalent, divalent and trivalent ions in aqueous solution; the characteristic potential E_p of the cathodic process depends upon the nature of the intercalated cation. Electrochemical measurements demonstrate the unprecedented fast kinetics of trivalent ion insertion associated with this material. The reported findings represent the first systematic step toward understanding the principles of multivalent charge screening and provide a novel cation intercalation mechanism in NiHCF, assisted by both water molecules and ferrocyanide vacancies. The synergistic mechanism can reduce the electrostatic repulsion and provide a preferential path for the rapid cation intercalation.

Keywords: alkali cations, cation exchange, ion sensing, nickel-hexacyanoferrate, trivalent cations.

1. INTRODUCTION

The development and study of electrochemical sensors, which offer interesting advantages of rapid and non-invasive analysis, has become an interesting area of research in recent years [1].

Chemically modified electrodes (CMEs) with Prussian blue analogues (PBAs) have been successfully employed in ion-sensing applications to introduce highly selective electrode responses [2].

PBAs belong to a class of important coordination complexes exhibiting interesting redox chemistry accompanied by changes in their electroanalytical, electrochromic, ion-exchange and electrocatalytic properties [2-5]. These solid compounds of mixed valence present general formula: $A_xM_y[B(CN)_6] \times nH_2O$ where M and B are transition metals, A an alkaline metal, x and y stoichiometric coefficients, n the hydration-intercalation molecules per unit formula (≤ 14).

Their reactions involve the insertion of metal ions into the zeolite-like, open structure consisting of a cubic network of iron centers bound by cyanide bridges.

The exchange of alkali cations during the redox reactions is the basis for the ion selectivity of these compounds. Metal-hexacyanoferrates, or PBAs, can be described in the “soluble” and the “insoluble” form (these terms were assigned historically according to their intrinsic property of forming colloidal solutions); the most important difference between them is the lack of one-fourth of the $B(CN)_6^{3-}$ units, replaced by coordinated and non-coordinated water molecules, in the “insoluble” form. However, it is worth noting that PB analogs are insoluble in water.

Among PBAs, nickel(II) hexacyanoferrate(II,III), NiHCF, [6,7] is interesting because of several technological applications, such as charge storage [8-14], electroanalysis [15], electrocatalysis [16-18], ion exchange [19-22] and chemical sensor [2, 23-26] including biochemical and electrochemical sensing.

NiHCF films are synthesized by electrochemical deposition on different electrodes through potential cycling [27, 28] of macro-molecular crystal structures. The overall stoichiometry of the electroformed films is strongly related to the electrodeposition conditions [29].

Nickel-hexacyanoferrate is characterized by well-defined, reversible and reproducible responses in different supporting electrolytes; its electrochemical behavior depends selectively on the type and on the concentration of the cation [30]. Bocarsly and coworkers showed cyclic voltammograms for anodically derivatized NiHCF films cycled in various alkali cation solutions and they noted that the selectivity for the alkali cations of interest increases in the order $Na^+ < K^+ < Cs^+$ [31, 32].

Nickel-hexacyanoferrate represents an excellent candidate for separations involving alkali cations as proved in the literature [33-36] and its capability to reversibly exchange many monovalent and divalent ions attracted interest for new energy storage systems design.

The requirement for electrochemical energy storage in the form of secondary batteries continues in parallel with the efforts to provide higher power, higher energy density, lower cost, safe and longer cycle life electrode materials.

Nowadays, lithium ion batteries are considered one of the most interesting technologies for large-scale energy storage systems due to their high energy density (472 Wh kg^{-1}), and long lifetime. However, the abundance of terrestrial reserves of lithium is limited and with unequal geographic distribution, furthermore the lithium recycling is difficult and it has high price and low sustainability. As a result, many efforts have been made to research novel efficient and lower cost electrochemical energy storage systems.

Hence, nowadays the use of sodium-ion batteries particularly for large scale energy storage attracted great attention due to the large availability and low cost of sodium.

However, if a “guest ion” can move two or three charges (i.e. multivalent ions can carry an higher electric charge than monovalent ones), the insertion reaction should store more energy than that of Li or Na ion batteries. An important aspect to underline is the ion mobility within the host materials, that is highly dependent on the charge and the size of the guest ion.

Several studies have been performed to investigate new potential cathode and anode materials; a key issue is the enough large channel structure to make adapt the diffusion and storage of the multivalent ion.

Our experiences with the solid state electrochemistry of metal-hexacyanometallates and success with monovalent and divalent ion insertion made us question whether it would be possible to intercalate trivalent cations within the metal-hexacyanometallate lattice and motivated us to explore these materials also for trivalent insertion. While divalent ions have been shown to reversibly insert with long cycle life into nickel-hexacyanoferrate [37] and PB thin films, suggesting that divalent alkaline earth cations (Mg^{2+} , Ca^{2+} , Sr^{2+} , Ba^{2+}) can reversibly insert into these materials [38, 39], no work demonstrates insertion of a range of trivalent ions in nickel-hexacyanoferrate.

In this paper, our group reported a detailed electrochemical study about the insertion/de-insertion of trivalent cations in NiHCF lattice in addition to an accurate study of the effects of different monovalent cations. The obtained results provide a novel intercalation mechanism in NiHCF, assisted by both water molecules and ferrocyanide vacancies, reducing the electrostatic repulsion and provide a preferential path for the rapid monovalent and multivalent cation intercalation.

Furthermore, findings confirm the exchangeability properties of NiHCF, useful in several technological applications including wastewater treatment, energy-storage devices and element purification.

2. EXPERIMENTAL

2.1. Materials

Chemicals were reagent grade from Sigma-Aldrich ($K_3Fe(CN)_6$, $Ni(NO_3)_2$, KNO_3 , $NaOH$, $LiOH$, $CsOH$, $Al(NO_3)_3$, $Cr(NO_3)_3$, $In(NO_3)_3$, $Gd(NO_3)_3$, $Er(NO_3)_3$) and used without any further purification.

All experiments have been performed in air, at room temperature and with deionized water, except the dehydration of the sample carried on in oven at 70°C.

2.2. Apparatus

Electrochemical measurements were performed with a Model 660c (CH Instruments) electrochemical work station using a standard three-electrode electrochemical glass cell (10 ml). The substrate of the working electrode was glassy carbon, GC (diameter \approx 0.7 mm) or graphite foil, GF (0.10 mm thick, 99.9%, Goodfellow) or a gold plated plastic film, PG (electrode area of the electrodes

= 2 cm²) [40]; and a Pt counter electrode was used. All potentials were reported vs Ag/AgCl reference electrode in saturated KCl.

X-ray powder diffraction (XRD) patterns were acquired with the Mo K_α X-ray source equipped with a Huber goniometer. Diffraction patterns were collected between 5° and 70°, where most reflections of nickel-hexacyanoferrates diffraction patterns appear. The cell parameter, *a*, referred to the cubic structure, was obtained by pattern matching using the Unit Cell program as reported by Holland [41].

X-ray fluorescence (XRF) elemental analysis was performed with a Shimadzu 800HS.

2.3. Preparation of NiHCF-modified electrodes and electrochemical measurements

Before electrodepositing NiHCF, working electrodes (Ni metal, GF, or PG) were always pretreated by performing 20 cycles from 0.9 V to 0.0 V at 0.050 V s⁻¹ in 1.0 M KNO₃ solutions.

Subsequently, NiHCF films were deposited by dynamic electrodeposition through cyclic voltammetry (CV) scans in a 1.0 M KNO₃, 5.0×10⁻⁴ M K₃Fe(CN)₆ and 5.0×10⁻⁴ M Ni(NO₃)₂ solution between 0.9 V and 0.0 V.

The electrochemical behavior in presence of different monovalent and trivalent metal cations was investigated by recording CVs in various supporting electrolytes and following a precise protocol. In particular, for all the sequences, a first CV in KNO₃ electrolyte was followed by several CVs in the solution of chosen cation taken at different scan rates. To check the complete reversibility of cation intercalation, the last CV was accomplished in KNO₃ initial solution.

2.4. NiHCF chemical deposition

Nickel-hexacyanoferrate powders containing K⁺ were synthesized by a simple coprecipitation method and in particular by dropwise addition, at room temperature, of equimolar amounts of K₃Fe(CN)₆ water solution to a precursor Ni(NO₃)₂ solution (typically 0.1 M) under stirring. A green colloidal solution, characteristic of NiHCF compound, was obtained as soon as the solutions of both the precursors were in contact. To improve the polymerization, the solution was allowed to stand for a night to enable the deposition of the product. Subsequently, the sample was carefully washed with deionized water in order to remove the unreacted salts and centrifuged to separate the solid product. Finally, the precipitate was dried at 70°C.

XNiFe(CN)₆ samples used for X-Ray diffraction measurements (where X = Na, Li or Cs) were precipitated from H₃Fe(CN)₆, obtained from K₃Fe(CN)₆ precursor, by ion exchange on a column packed with Amberlite IR 120 plus resin from Aldrich. The ferricyanic acid was neutralized by the hydroxide of the desired cation (NaOH, LiOH, CsOH) to form the corresponding ferricyanide. Subsequently, the obtained hexacyanoferrate was mixed by dropwise addition to an equivalent amount of Ni(NO₃)₂, and finally the solid product was centrifuged and dried at 70°C.

3. RESULTS AND DISCUSSION

The study deals with the influence of two different supporting electrolytes containing either potassium or sodium, during the nickel-hexacyanoferrate electrodeposition.

NiHCF was electro-formed on various substrates, Ni metal, graphite foil, GF, and plastic gold, PG, (depending on the further applications) by cyclic voltammetry (CV), as reported in detail in the Experimental section.

Briefly, the formation of NiHCF was achieved in the potentiodynamic mode in solution containing either KNO_3 or NaNO_3 both 1.0 M as supporting electrolyte and equimolar (5.0×10^{-4} M) $\text{Ni}(\text{NO}_3)_2$ and $\text{K}_3\text{Fe}(\text{CN})_6$ water solutions.

During the cycling process, the peak current intensity increased depending on the number of scans leading to the growth of the NiHCF film during the CV scans. It is worth noting that NiHCF and Prussian Blue analogs, are known to grow in a *fcc* cubic crystal structure, described in the “soluble” and the “insoluble” form, as previously reported.

At the end of the electrodeposition process, three CVs were performed in the supporting electrolyte solution in order to verify the formation of NiHCF film by the presence of reproducible CVs and characteristic redox peaks. Figure 1 shows the last CV for NiHCF-modified electrode in a supporting electrolyte containing K^+ (black line) and Na^+ (red line) respectively.

Nickel-hexacyanoferrate contains electrochemically reversible iron centres that switch between reduced Fe(II) and oxidized Fe(III) states depending on the applied voltage.

The redox activity of NiHCF film arises from the electron transfer to or from the iron synergistically to the displacement of K^+ ions from the lattice; the transfer of cations between the electrode surface and the solution interface is required to maintain charge balance.

NiHCF films have a zeolite-like network structure of electroactive sites placed inside the porous structures and its electrochemical activity was found in previous studies to be dependent on synthetic protocols, crystal structure and post-activation process, where these parameters also have an effect on the current response of these modified electrodes [38].

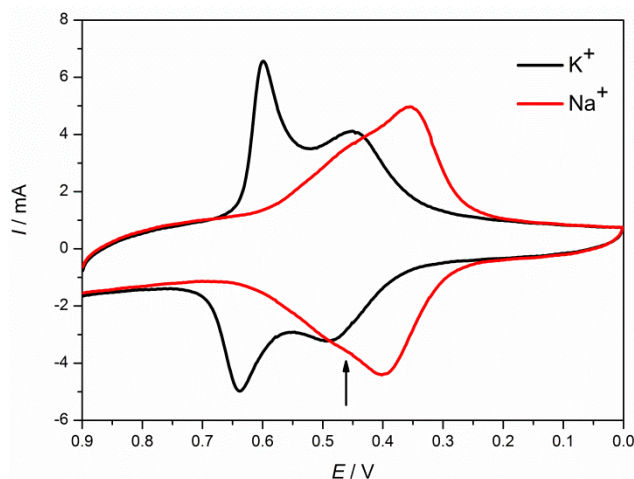


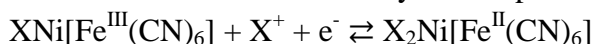
Figure 1. CV of a NiHCF film electrodeposited on PG in a supporting electrolyte containing Na^+ (red line) and K^+ (black line) in potentiodynamic mode at 0.1 V s^{-1} scan rate and in the potential range from 0.9 to 0.0 V

Regardless the electrode substrates, typical CV obtained by using K^+ as supporting electrolyte (black line in Fig. 1) shows the typical shape of bulk NiHCF [42] with the presence of two redox couples at about 0.63 V vs Ag/AgCl (in addition to smaller peaks at about 0.45 V), as well described in the literature.

The presence of two peaks should be attributed to the existence of two stable forms, both electroactive, and the peak at more positive potentials can be attributed to the predominant K^+ presence [43].

As concern a supporting electrolyte containing Na^+ , unlike K^+ , the CV resulting from the electrodeposition shows only one reversible redox couple at lower potential. A closer inspection of the reduction and oxidation process reveals a shoulder (indicated in Figure 1 by an arrow) at 0.46 V vs Ag/AgCl reference electrode.

In these cases, the electrochemical reaction takes place with a cation insertion and de-insertion in order to ensure the electro-neutrality of the species and can be written in the simplified version as



(1)

regardless the nature of the inserted alkali cation X and the presence of more complex reduction paths.

No trace of the electroplating solution was retained by the film after rinsing as confirmed by the absence of the ferricyanide redox peaks in the cyclic voltammogram. Hence, on the basis of reaction (1), it is possible to exchange the native alkali cation with another one.

The coverage of the electrode shown in Table 1, and the results shown hereafter, are referred to the glassy carbon (GC) electrode. In particular, the values were calculated integrating the current after 3, 6, 9 cyclovoltammetric deposition steps assuming the cell parameter, a , determined by pattern matching, equal to 10.2 Å, that is in the typical value of most metal-hexacyanometallates.

Table 1. Calculated coverage of the electrode surface, understood to mean the thickness of the NiHCF film electrodeposited on the glassy carbon.

Voltammetric cycles	Layers number	Thickness/cm
3	153.27	1.5634×10^{-5}
6	202.94	2.07×10^{-5}
9	435.05	4.4375×10^{-5}

The properties of NiHCF films and the presence of one or two redox couples are dependent upon the conditions of the electrosynthesis, and in particular upon both the electrodeposition time and the scan rate, as observed in the literature from Zamponi [42].

It is worth highlighting that the NiHCF deposition is performed on different electrodic substrates (i.e. GC, PG and GF) and the resulting CVs show the same morphology and peak potentials. The electrochemical behavior in presence of different monovalent metal cations was investigated by recording CVs in various supporting electrolytes, namely Na^+ , K^+ , Li^+ , and Cs^+ .

As detailed in the Experimental section, a first CV taken in KNO_3 electrolyte was followed by several CVs in the solution of chosen cation recorded at different scan rates. To check the complete reversibility of cation intercalation, the last CV was accomplished in KNO_3 initial solution. This novel protocol allows to check the reversibility of the process and hence the evaluation of the affinities of the test cations relative to that of K^+ .

The results are shown in Fig. 2 a, b and c for Li^+ , Na^+ and Cs^+ respectively. The replacement of K^+ ions with another cation causes considerable changes in the peak position and shape.

As noted previously for other Prussian Blue analogs, the shift in the peak potential relates to the ionic potential of the cation, or it may be due to the developing of new modified sites, as reported in the literature [44].

When the final experiment in the solution containing 1.0 M KNO_3 is performed after testing in different supporting electrolytes, the obtained CV morphologies are similar to the initial one in KNO_3 . The intensities in the final experiment are slightly reduced, as expected for loss of the electroactive material.

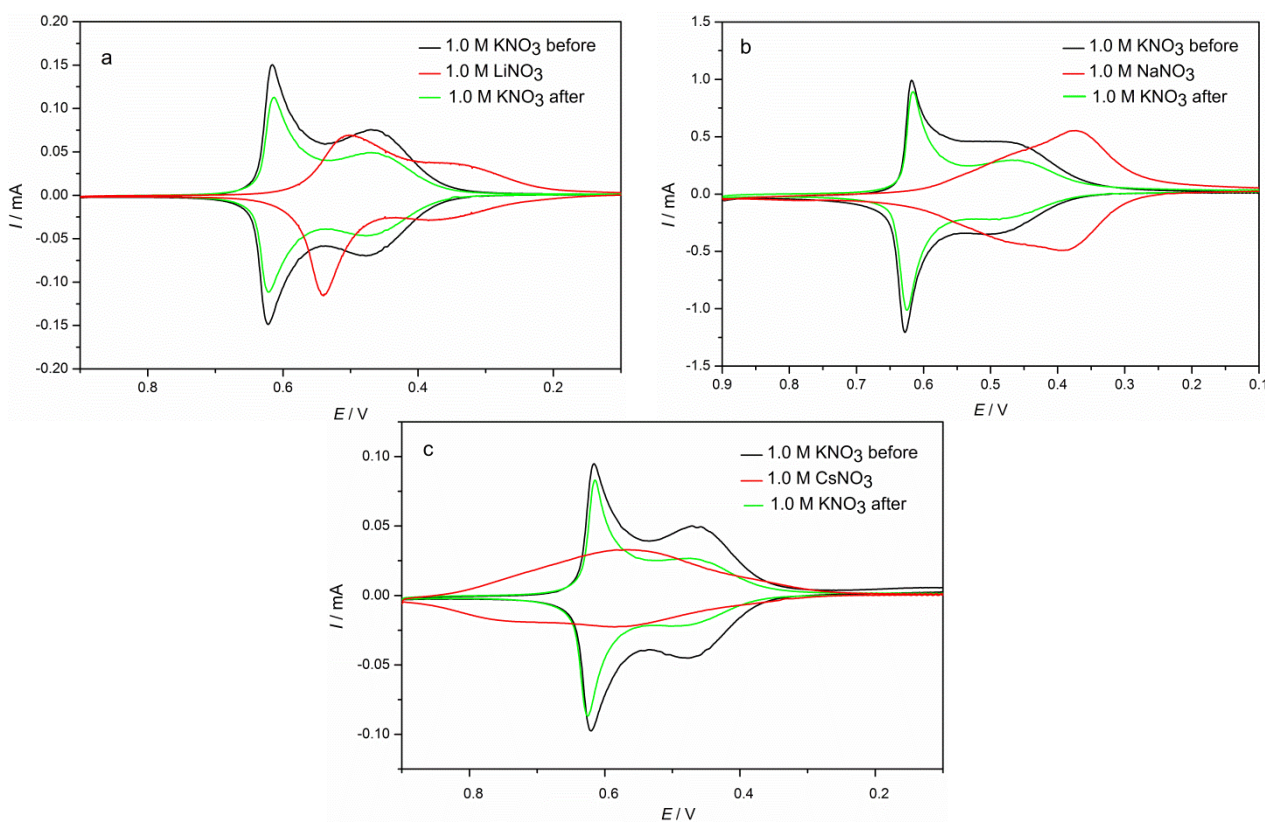


Figure 2. CVs of NiHCF films in a) 1.0 M LiNO_3 , b) NaNO_3 and c) CsNO_3 solutions at 0.1 V s^{-1}

Figure 3 shows a synoptic cyclic voltammogram resulting in different alkali metal cation electrolyte. It is worth noting that all the modified GC electrodes investigated in the paper, have the same area.

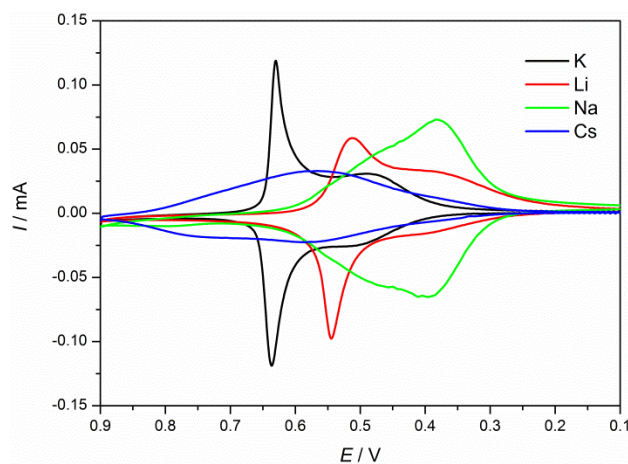


Figure 3. CVs of NiHCF film cycled in 1.0 M KNO_3 , NaNO_3 , LiNO_3 and CsNO_3 supporting electrolyte solutions (scan rate = 0.1 V s^{-1}) and in the potential range from 0.9 to 0.0 V

Cyclic voltammograms (CVs) demonstrate reversible insertion of all the investigated cations in NiHCF, however, only small broad peaks and one pair of ill-defined redox peaks were observed in Cs solutions. Both the insertion voltages and the qualitative shapes of the CVs vary significantly as a function of the insertion ion. NiHCF voltammetric responses yield single sets of peaks in lithium and sodium electrolytes, reflecting the lower abilities of hydrated Li^+ and Na^+ to undergo ion pairing with metal-hexacyanoferrates [45].

It is worth noting that although the same electrochemical process is evidenced in the NiHCF film, the presence of multiple cathodic and anodic peaks at different voltages in the data may suggest the presence of multiple electrochemical active sites during the ion intercalation.

The above results highlight the greater selectivity of NiHCF towards K^+ ions as a counter-cations, in fact when the NiHCF modified electrode is cycled in solutions containing Na^+ , Li^+ and Cs^+ , a slight decrease of the amount of Q charge is calculated, compared with those studied in K ones.

However, the original performances are mostly restored when the electrode with the foreign cation is cycled in 1.0 M KNO_3 solution.

It is worth noting that both the previously reported protocol and the kinetic study highlight a notable thermodynamic and kinetic reversibility related to the investigated cations, most of all for potassium and lithium, and an evident decrease of the insoluble species, especially shown by using a solution containing lithium.

In particular, the intercalation kinetics relative to the different monovalent cations have been explored by CVs performed with scan rates in the $0.001\text{--}0.500 \text{ V s}^{-1}$ range in 1.0 M solutions.

As concern lithium, potassium and cesium the peak heights result linearly dependent upon the scan rate at low scan rates and dependent upon the square root of the scan rate at high scan rates, following the Randles-Sevcik equation.

At high scan rates values, the limiting factor is the supply of the monovalent cation at the electrode/solution interface (indicating a semi-infinite linear diffusion) while at low scan rates the limiting factor becomes the diffusion rate of the monovalent cation in NiHCF. In this second case, a surface-confined electrochemical process is observed. Conversely, the regime is different for sodium

ions, since the peak heights were linearly dependent upon the scan rate both at low and high scan rates indicating that a surface-confined electrochemical process occurs. It is worth noting an evident increase of the insoluble species when sodium cations are used as counter-cations to balance the charge in NiHCF lattice. Furthermore, by plotting the peak current vs the scan rates values, it is possible to obtain higher slope values for lithium and potassium than that observed for sodium and cesium, highlighting a more facile and fast intercalation process for the first two cations and more sluggish kinetics for the other ones.

The peak separation, $\Delta E_p = E_{pa} - E_{pc}$ became wider at higher scan rates than at lower scan rates, indicating a limitation arising from slower charge transfer kinetics. These results suggest that the reaction kinetics change from a surface process to a diffusion-controlled process.

In order to understand the behavior of NiHCF in solution containing alkaline cations, the hydrated radius size and the Gibbs energy of hydration of the investigated metal cations are analyzed.

The hydrated radii of the studied alkali metal cations are 340, 276 and 232 pm for Li^+ , Na^+ and K^+ respectively, and from geometrical considerations, the NiHCF cavity radius is about 500 pm.

It is possible to hypothesize that the counter-cations undergo a partial dehydration to enter the crystal lattice. The experimental Gibbs energy of hydration for Li, Na and K is -477, -371 and -300 kJ mol⁻¹, respectively [46]. It is worth noting the higher the Gibbs energy of hydration, the more difficult is the dehydration. Thus, the hydrated Li undergoes the smallest extent of dehydration of the above three cations (Li^+ , Na^+ and K^+) and it is the most difficult one to be exchanged into the film. As concern the CVs in lithium, it is worth noting the intensities in the final experiment in KNO_3 are more reduced than the Na^+ and K^+ ones, as proved by the great decrease of the electrochemical active sites related to the insoluble species.

Ions with smaller crystal radii have higher hydration numbers and larger hydrated radii, hence they maintain their hydration shells more strongly. On the other hand, ions with larger crystal radii have weaker hydration shells, hence, they may be able to detach from their hydration layer while passing through the NiHCF lattice.

The small hydrated cations, such as Cs^+ need a separate discussion. Cs^+ ion provide low currents spreading over a wide potential range in the CV, as observed in Fig. 3. As reported by Dostal [47] in the literature, this different issue is due to its ability to induce microstructural distortions probably caused by a reduced mobility of Cs^+ ion in the NiHCF lattice channel.

Considering these experimental results and depending on the insoluble or soluble species, the cation can occupy different possible interstitial sites in NiHCF cubic structure, as shown in Fig. 4 a and b.

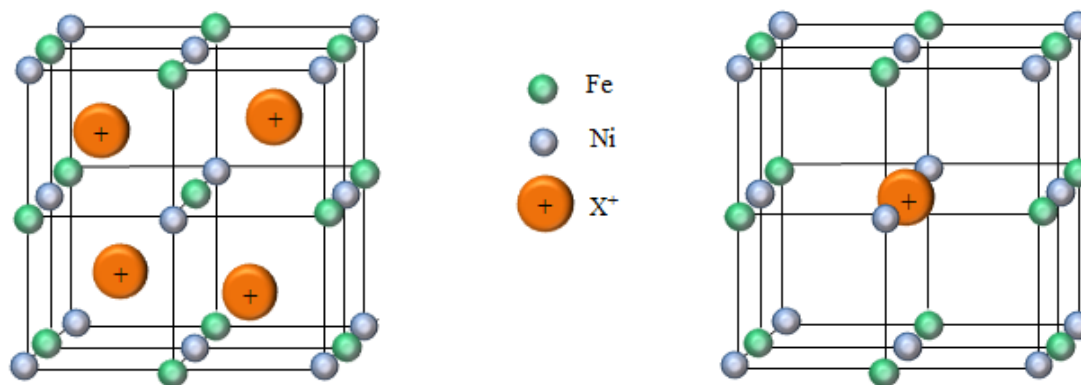


Figure 4. NiHCF structure analog to “soluble” Prussian Blue on the left and analog to “insoluble” Prussian Blue on the right. The orange spheres indicate monovalent cations intercalated into the tetrahedral cavities of the lattice to neutralize the charge of the system

The structure on the left (Fig. 4a) is analog to “soluble” Prussian Blue, providing an ordered rigid structure while the structure on the right, analog to “insoluble” Prussian Blue, includes vacancies of the $\text{Fe}(\text{CN})_6^{3-}$ group, hence it results featured by a more flexible cubic framework.

The stoichiometry of NiHCF and its elemental composition was determined using X-ray fluorescence spectroscopy (XRF) and the Ni/Fe stoichiometric ratio points to the so called “insoluble” form, rich in vacancies of the $\text{Fe}(\text{CN})_6^{3-}$ group.

3.1 Structural information by XRD measurements

Important data are provided by XRD measurements reported in Fig. 5, demonstrating the insertion of all the investigated monovalent ions in the structure and his crystalline structure.

The diffractogram confirms the success of NiHCF synthesis and allow the identification of lattice changes in the structure when different cations are intercalated.

XRD patterns reported in Fig. 5 referred to the samples obtained by chemical synthesis, are consistent with the typical *fcc* lattice of metal-hexacyanoferrates and the major characteristic peaks can be assigned as (200), (220), (400) and (420) crystal planes, as observed in the most of PB analogs. In the XRD diffraction pattern of potassium and sodium, the strongest reflection peaks are the (200), missing in the cesium lattice, as already shown in the literature by Kelly [48].

NiHCF structure is retained in all the investigated monovalent cations, although a shift in the peak positions occurs. Slight lattice changes are probably due to the higher radius of these cations compared to the potassium one, bringing negligible stress variation (close to zero-strain characteristic) within the intercalation/de-intercalation processes, which minimizes the structural instability providing an excellent cyclic stability.

In addition, it could be hypothesized that multiple peaks in the cyclic voltammograms correspond to ions intercalation into these electrochemically distinct sites in the NiHCF structure, as shown below.

It is worth highlighting that the morphology of the cyclic voltammogram and the peak potentials of NiHCF modified electrodes, containing the different monovalent alkali cations, both chemically and electrochemically, result the same.

Furthermore, the elemental analysis of the compounds not containing potassium (performed by X-ray fluorescence spectroscopy), confirms the ability of the ion-exchange resin, Amberlite, to perfectly exchange potassium, allowing to obtain pure compounds containing the desired investigated cation.

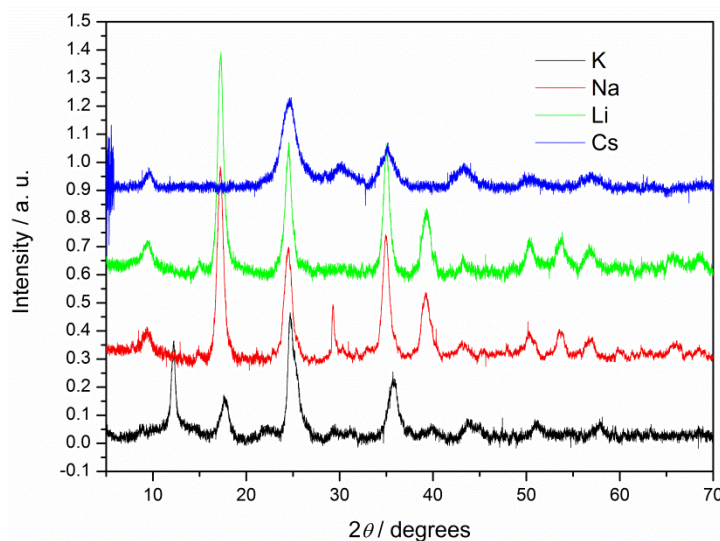


Figure 5. X ray diffrattograms of NiHCF powders containing all the investigated monovalent ions, K⁺, Na⁺, Li⁺, Cs⁺

The present understanding of cation intercalation in metal-hexacyanoferrates doesn't provide a complete explanation for why electrochemical properties vary considerably with the different intercalated cation. Rietveld refinement results reported in the literature [49] and our studies suggest that both water molecules and vacancies could provide cation intercalation; the detailed mechanism relative to the cation intercalation in metal-hexacyanoferrates is a topic of ongoing study.

Rassat [34] underline that metal-hexacyanoferrates are commonly used as ion exchangers, but the stability of these materials is not checked, because they are tested only once.

The stability of the film by repeated CV scans at 0.1 V s⁻¹ was checked. The intensity of the cathodic peak current, I_{pc}, decreases monotonically with the number of cycles and reduces to 10% after 100 cycles. This phenomenon may be probably due to loss of electroactive material.

Extended cycling of monovalent ions over 100 cycles demonstrates the high structural integrity of NiHCF even after such extended cycling. No change in crystal structure or decrease in crystallinity after cycling is observed.

As a matter of fact, for all the investigated monovalent cations, no partial substitution of the Ni atom coordinated to the nitrogen atom is provided by the alkaline cations, contrary to what is the Prussian Blue behavior [50] where i.e. Ni²⁺ and Cd²⁺ atoms can partially replace the iron coordinated to nitrogen atom.

The perfect electrochemical reversibility confirms the absence of any substitution of Ni, in the time scale of the experiments; however, the kinetic process may be too slow to be detected. Further experiments will be required in order to evaluate this hypothesis.

3.2 Trivalent cations intercalation in nickel-hexacyanoferrate films

Our experience with the solid state electrochemistry of metal-hexacyanometallates made us question whether it would be possible to intercalate divalent or trivalent cations within the NiHCF lattice. Divalent ions have been shown to reversibly insert with long cycle life into nickel-hexacyanoferrate as reported by Wang [17, 37]. The radii of all these hydrated cations are larger than that of K^+ and the hydration energy of the alkaline earth metal cations is greatly larger compared to Li^+ cation. Wang hypothesized that the presence of hydrated ions and water molecules throughout the structure, may shield electrostatic interactions during diffusion analogously to water molecules assisting Mg^{2+} intercalation in V_2O_5 electrodes [51].

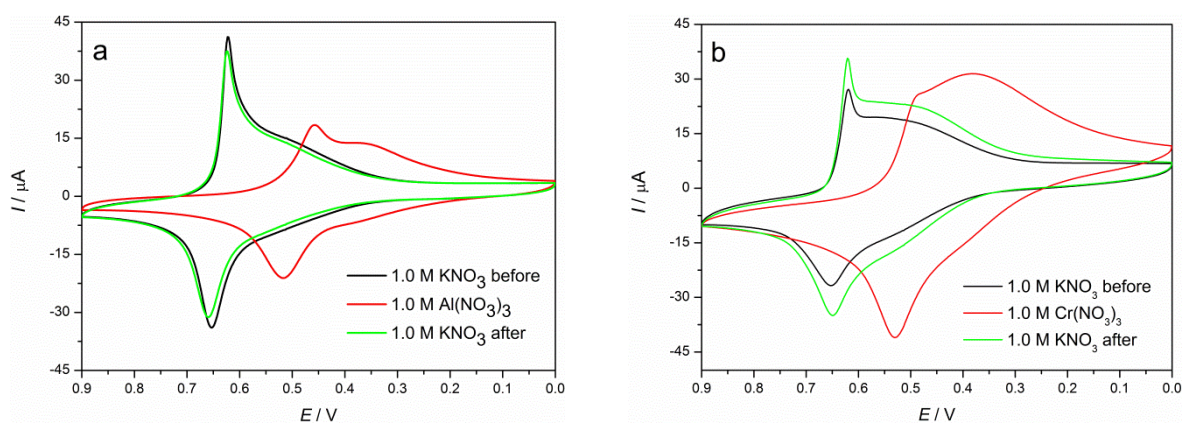
Here the paper expanded upon the previous works reporting the insertion of a wide variety of trivalent ions from the transition metal and rare earth families in nickel-hexacyanoferrate providing an understanding of aspects of the electrochemical performance.

The electrochemical behavior in presence of different trivalent metal cations was investigated by recording CVs in various supporting electrolytes, namely Al^{3+} , Cr^{3+} , In^{3+} , Gd^{3+} and Er^{3+} following the previous reported protocol.

In particular, a CV was initially performed in a 1.0 M KNO_3 solution; a second CV was subsequently recorded in a 1.0 M solution of trivalent cation, and finally the last cyclic voltammetry scan was replicated when the electrode was returned to the native solution containing K^+ ions.

The results are shown in Fig. 6a, b, c, d and e for Al^{3+} , Cr^{3+} , In^{3+} , Gd^{3+} and Er^{3+} respectively. The replacement of K^+ ions with a trivalent cation causes changes in the peak position and shape, as shown for monovalent cations.

When the final experiment in 1.0 M potassium nitrate is performed after testing in solutions with the trivalent cations, CVs morphologies are the same compared to the original one in KNO_3 , highlighting a perfect reversibility.



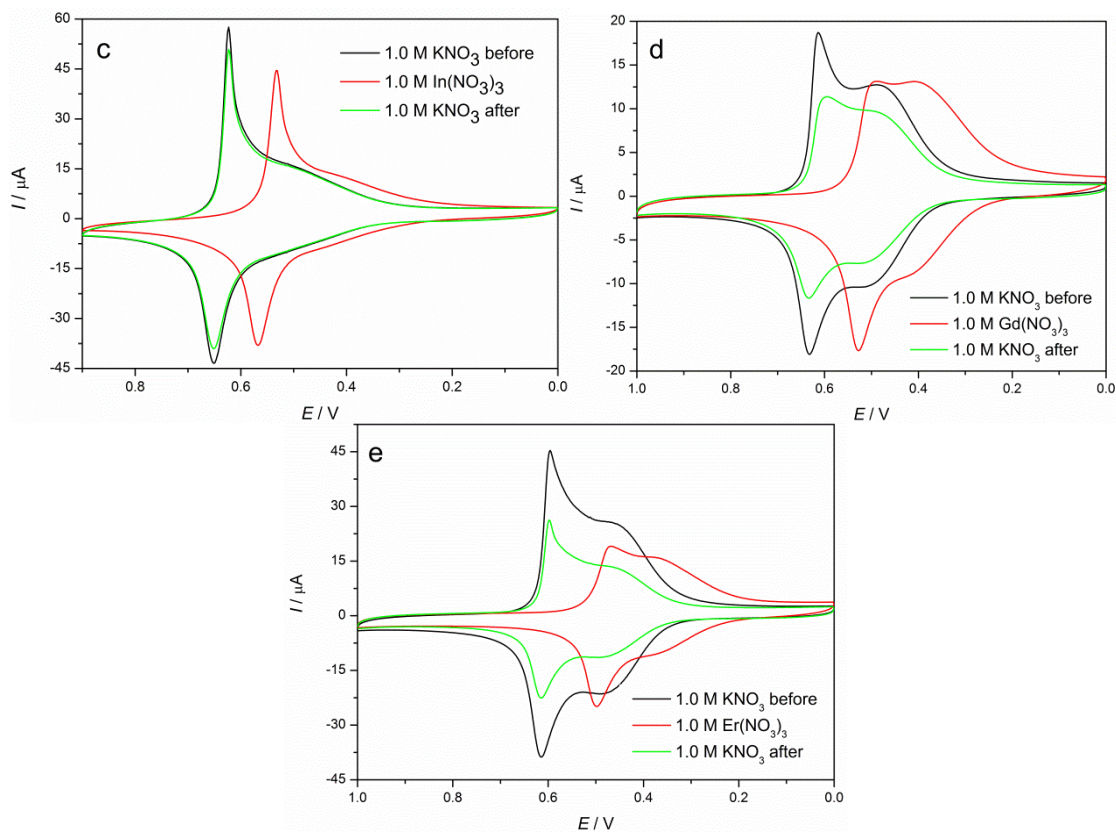


Figure 6. CVs of NiHCF films in a) 1.0 M Al^{3+} , b) Cr^{3+} , c) In^{3+} , d) Gd^{3+} and e) Er^{3+} solutions at 0.1 V s^{-1}

As observed for monovalent cations, also in trivalent ones, the intensities in the final experiment are reduced, probably due to the loss of the electroactive material, most of all as concern the rare earth elements.

CVs morphology of rare earth elements are strikingly similar (Fig. 6d and e), which reflects the chemical similarity of the rare earth elements.

Counterintuitively, the oxidation state increase of the insertion ion from +1 to +3 induces a trivial effect on insertion electrochemistry in NiHCF compound. In the most of materials, the charge state represents the critical factor of electrochemical intercalation.

These considerations may evidence the key role of water molecules, either in the structure or in the hydration shell that reduce the electrostatic interaction between the insertion ion and the host ions in the NiHCF lattice, providing a water-mediated cation intercalation and resulting in a remarkable charge screening.

The intercalation is intensely influenced by the hydrated radii of the inserted trivalent cations or at least partially hydrated, allowing rapid and reversible insertion kinetics of trivalent ions through the channels.

Hence, a possible suggestion is that trivalent ions require additional hydration to remain in the structure. It is not completely clear if hydrated ions can be intercalated through different pathways, like the ferricyanide vacancy paths [52], if the ion hydration concerns only alongside the axes during diffusion [53] or if both mechanisms provide the cation intercalation in nickel-hexacyanoferrate lattice.

The stoichiometry of the compounds and the elemental compositions were determined using X-ray fluorescence spectroscopy (XRF) and it is worth underlining that Ni/Fe stoichiometric ratio approaches the limit value (1.8) of the so called "insoluble" form, rich in vacancies of the $\text{Fe}(\text{CN})_6^{3-}$ group, and it is far from 1, characteristic value of the so called "soluble" form.

Ferricyanide vacancies size, which are approximately 5 Å in diameter and larger than the 3.2 Å interstitial sites (shown in Fig. 4), could assist insertion by providing additional diffusion paths for insertion ions.

As concern solutions containing trivalent cations, the protocol and the kinetic study highlight a notable thermodynamic and kinetic reversibility related to the investigated cations, most of all for Al^{3+} cation, showing unprecedented electrochemical performance.

Furthermore, CVs performed in solutions containing trivalent cations show multiple anodic and cathodic peaks at well-defined voltages, compatible with cations intercalation into different distinct crystallographic sites, according to the electrochemical results obtained at different scan rates shown in Fig. 7, and confirming different dehydration degrees in the intercalation process [52].

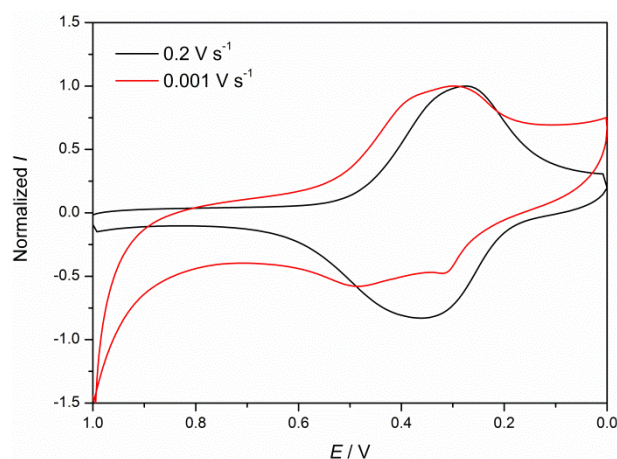


Figure 7. CVs of NiHCF film recorded in 1.0 M $\text{Cr}(\text{NO}_3)_3$ solution at 0.2 V s^{-1} (red line) and 0.001 V s^{-1} (black line)

Changes in intercalation voltage and kinetics of different trivalent cations reflect the complicated mechanisms occurring during trivalent cations intercalation, providing a field of study in progress.

The reported experiments are among the first systematic steps toward understanding the principles of charge screening providing a novel cation intercalation mechanism assisted by ferrocyanide vacancies. The synergistic mechanism can reduce the electrostatic repulsion and provide a preferential path for the rapid cation intercalation.

Hence the results suggest a new approach to multivalent cation intercalation that could help to advance the understanding of these complex mechanisms.

4. CONCLUSIONS

The paper deals with a detailed electrochemical study about the insertion/de-insertion mechanism of trivalent cations in nickel-hexacyanoferrate lattice in addition to an accurate study of the effects of different monovalent cations.

Both physical and structural properties make NiHCF open framework materials ideal for reversible electrochemical intercalation of cations with different oxidation states, in particular of trivalent cations, as never reported before. Cyclic voltammograms demonstrate reversible intercalation of different monovalent and trivalent cations, also from the rare earth series of elements. Cyclic voltammograms morphologies are generally well defined and trivalent ions appear to insert gradually over a wider range of voltages. Each voltammogram exhibits multiple cathodic and anodic peaks suggesting a more complex intercalation mechanism with different thermodynamically distinct intercalation sites for each cation. This could reflect the changes in the degree of dehydration required in order to intercalate cations into different sites within the lattice influencing also the mobility of alkali cations into the NiHCF structure.

A notable thermodynamic and kinetic reversibility related to the investigated cations, both monovalent and trivalent, most of all for potassium, lithium and aluminum is observed.

It is worth highlighting that regardless of the electrochemical synthesis route and of the supporting electrolyte used in the electrodeposition step, shapes and positions of the CV waves are strongly related to the cation of the electrolyte, which undergoes intercalation/de-intercalation during the redox process.

The versatility of the intercalation reaction in nickel-hexacyanoferrate may make this material appropriate for several applications including electrodes materials for batteries, wastewater treatment, ion sensing and separation.

References

1. M. Esteban and A. Castano, *Environ. Int.*, 35 (2009) 438.
2. N.R. de Tacconi, K. Rajeshwar and R.O. Lezna, *Chem. Mater.*, 15 (2003) 3046.
3. P.J. Kulesza, M.A. Malik, S. Zamponi, M. Berrettoni and R. Marassi, *J. Electroanal. Chem.*, 397 (1995) 287.
4. H. Dussel, A. Dostal and F. Scholz, *Fresenius J. anal. Chem.*, 355 (1996) 21.
5. M. Ciabocco, M. Berrettoni, S. Zamponi, J.A. Cox and S. Marini, *J. Solid State Electrochem.*, 17 (2013) 2445.
6. A.B. Bocarsly and S. Sinha, *J. Electroanal. Chem.*, 137 (1982) 157.
7. S. Sinha, B.D. Humphrey and A.B. Bocarsly, *Inorg. Chem.*, 23 (1984) 203.
8. C.H. Li, Y. Nanba, D. Asakura, M. Okubo and D.R. Talham, *RSC Adv.*, 4 (2014) 24955.
9. S. Ghasemi, R. Ojani and S. Ausi, *Int. J. Hydrogen Energy*, 39 (2014) 14918.
10. Wang and Q. Chen, *ACS Appl. Mater. Interfaces*, 6 (2014) 6196.
11. A. Safavi, S.H. Kazemi and H. Kazemi, *Electrochim. Acta*, 56 (2011) 9191.
12. R.Y. Wang, C.D. Wessells, R.A. Huggins and Y. Cui, *Nano Lett.*, 13 (2013) 5748.
13. Y. Yue, Z. Zhang, A.J. Binder, J. Chen, X. Jin, S.H. Overbury and S. Dai, *Chem. Sus. Chem.*, 8 (2015) 177.
14. S. Yu, Y. Li, Y. Lu, B. Xu, Q. Wang, M. Yan and Y. Jiang, *J. Power Sources*, 275 (2015) 45.

15. M.H. Mashhadizadeh, T. Yousefi and A.N. Golikand, *Electrochim. Acta*, 59 (2012) 321.
16. A.S. Kumar, P. Barathi and K.C. Pillai, *J. Electroanal. Chem.*, 654 (2011) 85.
17. P. Prabhu, R. Suresh Babu and S. Sriman Narayanan, *Sens. Actuators B*, 156 (2011) 606.
18. N.S. Sangeetha and S. Sriman Narayanan, *Anal. Chimica Acta*, 828 (2014) 34.
19. T. Vincent, C. Vincent, Y. Barré, Y. Guari, G. Le Saout and E. Guibal, *J. Mater. Chem. A*, 2 (2014) 10007.
20. S. Karnjanakom, Y. Ma, G. Guan, P. Phanthong, X. Hao, X. Du, C. Samart and A. Abudula, *Electrochim. Acta*, 139 (2014) 36.
21. C.-Y. Chang, L.-K. Chau, W.-P. Hu, C.-Y. Wang and J.-H. Liao, *Microporous Mesoporous Mater.*, 109 (2008) 505.
22. S. Liao, C. Xue, Y. Wang, J. Zheng, X. Hao, G. Guan, A. Abuliti, H. Zhang and G. Ma, *Sep. Purif. Technol.*, 139 (2015) 63.
23. R.J. Mortimer, P.J.S. Barbeira, A.F.B. Sene and N.R. Stradiotto, *Talanta*, 49 (1999) 271.
24. D.R. Coon, L.J. Amos and A.B. Bocarsly, *Anal. Chem.*, 70 (1998) 3137.
25. J.Q. Ang, B.T.T. Nguyen and C.-S. Toh, *Sens. Actuators B*, 157 (2011) 417.
26. N. Bagkar, C.A. Betty, P.A. Hassan, K. Kahali, J.R. Bellare and J.V. Yakhmi, *Thin Solid Films*, 497 (2006) 259.
27. M.A. Malik, K. Miecznikowski and P.J. Kulesza, *Electrochim. Acta*, 45 (2000) 3777.
28. L.F. Schneemeyer, S.E. Spengler and D.W. Murphy, *Inorg. Chem.*, 24(1985) 3044.
29. M.A. Malik, P.J. Kulesza, R. Marassi, F. Nobili, K. Miecznikowski and S. Zamponi, *Electrochim. Acta*, 49 (2004) 4253.
30. T. Shibata and Y. Moritomo, *Chem. Commun.*, 50 (2014) 12941.
31. A. B. Bocarsly and S. Sinha, *J. Electroanal. Chem.*, 140 (1982) 167.
32. K. M. Jeerage, W. A. Steen and D. T. Schwartz, *Langmuir*, 18 (2002) 3620.
33. K. M. Jeerage and D. T. Schwartz, *Sep. Sci. Technol.*, 35 (2000) 2375.
34. S. D. Rassat, J. H. Sukanto, R. J. Orth, M. A. Lilga and, R. T. Hallen, *Sep. Pur. Technol.*, 15 (1999) 207.
35. L. J. Amos, A. Duggal, E. J. Mirsky, P. Ragonesi, A. Bocarsly and P. A. Fitzgerald-Bocarsly, *Anal. Chem.*, 60 (1988) 245.
36. K.M. Jeerage, Characterization of Electrodeposited Nickel Hexacyanoferrate for Electrochemically Switched Ion Exchange; University of Washington; Seattle, WA, 2001.
37. R.Y. Wang, C.D. Wessells and R. A. Huggins , Y. Cui, *Nano Lett.*, 13 (2013) 5748.
38. S.-M. Chen, *J. Electroanal. Chem.*, 521 (2002) 29.
39. Y. Mizuno, M. Okubo, E. Hosono, T. Kudo, H. Zhou and K. Ohishi, *J. Phys. Chem. C*, 117 (2013) 10877.
40. P.J. Kulesza, S. Zamponi, M.A. Malik, M. Berrettoni, A. Wolkiewicz and R. Marassi, *Electrochim. Acta*, 43 (1998) 919.
41. T.J.B. Holland and S.A.T. Redfern, *Mineral Mag*, 61 (1997) 65.
42. S. Zamponi, M. Berrettoni, P.J. Kulesza, K. Miecznikowski, M.A. Malik, O. Makowski and R. Marassi, *Electrochim. Acta*, 48 (2003) 4261.
43. P.J. Kulesza, K. Brajter and E. Dabek-Zlotorzynska, *Anal. Chem.*, 59 (1987) 2776.
44. R. W. Murray, in A. J. Bard Ed. *Electroanalytical Chemistry Series* vol. 13.
45. J. Bácskai, K. Martinez, E. Czirok, G. Inzelt, P.J. Kulesza and M.A. Malik, *J. Electroanal. Chem.*, 385 (1995) 241.
46. Y. Won, *J. Phys. Chem. A*, 116 (2012) 11763.
47. A. Dostal, G. Kauschka, S.J. Reddy and F. Scholz, *J. Electroanal. Chem.*, 406 (1996) 155.
48. M.T. Kelly, G.A. Arbuckle-Keil, L.A. Johnson, E.Y. Su, L.J. Amos, J.K. M. Chun and A.B. Bocarsly, *J. Electroanal. Chem.*, 500 (2001) 311.
49. R.Y. Wang, B. Shyam, K.H. Stone, J.N. Weker, M. Pasta, H.-W. Lee, M.F. Toney and Y. Cui, *Adv. Energy Mater.*, 5 (2015) 1401869.

50. A. Dostal, M. Hermes and F. Scholz, *J. Electroanal. Chem.*, 415 (1996) 133.
51. P. Novák, R. Imhof, O. Haas, *Electrochim. Acta*, 45 (1999) 351.
52. S.I. Ohkoshi, K. Nakagawa, K. Tomono, K. Imoto, Y. Tsunobuchi and H. Tokoro (2010) *J. Am. Chem. Soc.*, 132 (2010) 6620.
53. F. Scholz and A. Dostal, *Angew. Chem. Int. Ed.*, 34 (1996) 2685.

© 2018 The Authors. Published by ESG (www.electrochemsci.org). This article is an open access article distributed under the terms and conditions of the Creative Commons Attribution license (<http://creativecommons.org/licenses/by/4.0/>).